Estimating Stem Water Content From Tower-Based L-Band Tomographic Radar Using a Single-Scattering Model of a Uniform Layer: A First in Situ Experiment

Theresa Leistner, Albert R. Monteith, *Member, IEEE*, Jose Gutierrez Lopez, and Lars M. H. Ulander, *Fellow, IEEE*

***Abstract*—Spaceborne synthetic aperture radar missions have the potential to estimate forest vegetation water content (VWC), but understanding the underlying scattering processes and their link to VWC is still limited. In this article, tower-based tomographic radar observations of a boreal forest at L-band are used to measure canopy-only backscatter. Results show that the latter is anticorrelated with stem water content. Time series of both canopy backscatter and attenuation were extracted and linked to in situ stem water content using a scattering model. Results show that the proposed canopy backscatter model effectively captures the diurnal and long-term variations in stem water content, with an RMSE of 4%. The estimated model coefficients indicate that the sensitivity of extinction to stem water content dominates over the sensitivity of volume backscatter to stem water content. Moreover, the attenuation time series and corresponding model resulted in a better agreement with an RMSE of 2%. However, attenuation requires a known concealed reference target in the forest which limits its use over extended areas. While the study is limited in scope and the model has not been validated for broader generalization, these findings offer preliminary insights into the sensitivity of L-band radar to forest VWC and may support future observational strategies.**

***Index Terms*—Boreal forest, forest backscatter, L-band, stem water content (StWC), vegetation water content (VWC).**

Nomenclature

AGB	Above ground biomass (kg/m^2).
StWC	Stem water content (m^3/m^3).
SWC	Soil water content (m^3/m^3).
VPD	Vapor pressure deficit (kPa).
VWC	Vegetation water content; volumetric water content of the vegetation layer (m^3/m^3).

Received 29 August 2025; revised 17 November 2025; accepted 25 December 2025. Date of publication 5 January 2026; date of current version 16 January 2026. This work was supported in part by the Swedish National Space Agency (Rymdstyrelsen) under Grant 2021-00109, in part by the Swedish Research Council (Vetenskapsrdet) under Grant 2019-05289, in part by the Swedish Research Council for Sustainable Development (FORMAS) under Grant 2020-01961. *(Corresponding author: Theresa Leistner.)*

Theresa Leistner, Albert R. Monteith, and Lars M. H. Ulander are with the Department of Space, Earth and Environment, Chalmers University of Technology, 41296 Gothenburg, Sweden (e-mail: theresa.leistner@chalmers.se).

Jose Gutierrez Lopez is with the Department of Forest Ecology and Management, Swedish University of Agricultural Science (SLU), 90183 Umeå, Sweden.

Digital Object Identifier 10.1109/JSTARS.2025.3650660

I. Introduction

FORESTS play a fundamental role in the global hydrological and carbon cycles, in particular, through processes, such as evapotranspiration and carbon dioxide, uptake from the atmosphere [1], [2]. However, obtaining accurate and high-resolution measurements of key forest hydrological variables over large spatial and temporal scales remains a considerable challenge [3]. While promising tools such as new spaceborne synthetic aperture radar (SAR) systems operating at L- and C-band frequencies exist, the complex relationships between forest water dynamics and radar observations are still poorly understood. In particular, one open question is what characteristics a spaceborne SAR mission must possess to make the inversion of forest backscatter to vegetation water content (VWC) feasible.

To address this, several radar tower experiments with fine temporal resolution have been conducted to investigate the relationship between radar signals and forest water content [4], [5], [6], [7], [8], [9], [10]. Clear diurnal cycles in backscatter variations have been observed in tropical [5] and boreal forests [8], [9], [10]. These variations are believed to be driven by daily changes in canopy VWC. Diurnal fluctuations in VWC stored in the bark [11], [12], [13] of trees and in the canopy of low vegetation [14] have been observed in multiple studies, showing a decrease in water content during the onset of transpiration in the morning, due to the depletion of internal water reservoirs, and an increase at night as these reservoirs are replenished.

Recently, BorealScat-2, a radar tower experiment with tomographic capabilities, was installed in a boreal forest in northern Sweden. With its high spatial and temporal resolution it is able to observe clear diurnal cycles in backscatter variations at P-, UHF-, and L-band [4], [10]. However, at L-band the backscatter variations observed with BorealScat-2 differ from earlier observations with BorealScat (2017–2020) and from patterns observed at P-band [4], [10]. Specifically, L-band backscatter peaks during the day, a behavior that contradicts the conventional expectation derived from the water cloud model [15], which assumes that backscatter is a monotonically increasing function of VWC.

For forests, different simplified scattering models have been used for biomass estimation at X-band [16], soil moisture retrieval within forests at P-band [17] and estimates of crown and stem water content (StWC) at L- and P-band [18].

In this study, we use a simplified scattering model based on [17] to: 1) establish a link between in situ StWC and tomographically extracted canopy backscatter at L-band; and 2) extract time series of StWC from the inversion of a canopy backscatter model and the inversion of an attenuation model. Section II details the processing of BorealScat-2 data and describes the ancillary datasets used. Section III presents the proposed backscatter model, along with the procedures for parameter estimation. Section IV discusses model performance, specifically the agreement between modeled and measured backscatter, and compares the time series of modeled and in situ StWC. Finally, Section V concludes this article and interprets the results in the context of forest hydrodynamics and outlines considerations for future spaceborne SAR missions.

II. Data

A. Study Area

The BorealScat-2 radar tower (see Fig. 1) is located within the Svartberget Experimental Forest in northern Sweden. The 50 m high tower observes a dense, mature stand which is a mix of pine (65%), spruce (32%), and birch (3%), approximately 100 years old, with trees having a mean height of 18 m, a dominant height of 24 m, and a mean stem diameter of 20 cm [10]. In close proximity to the tower lies the ICOS Svartberget Atmospheric and Ecosystem Station that includes a 150 m high greenhouse gas research tower [19]. Measurements of the radar tower started in summer 2022. In May 2024, a 5-m concealed reflector (CR) was also installed at a 100 m ground range distance from the radar tower. The CR is used to measure variations in forest canopy attenuation.

B. Radar Data

The BorealScat-2 radar tower acquires multilooked P-, UHF-, L-, and C-band vertical tomographic time series data at all linear polarization combinations with high backscatter precision every 30 min [4], [10]. Tomographic images are made possible by coherent measurements from a vertical array of 20 antennas at the top of the tower. Each antenna is connected to one port of a 20-port vector network analyzer (see Fig. 1), resulting in tomographic measurement times that are short enough for wind decorrelation to be neglected. Tomographic images were constructed using time-domain backprojection. Horizontal movement of the array over a 4 m aperture, and subsequent multilooking, provide more independent samples compared to a single image, improving backscatter precision. L-band vertical images at VV, HH, and cross-polarization were used to produce backscatter time series estimates by integrating intensity over a canopy region of interest. Cross polarization is here the intensity average of VH and HV.

Fig. 2 shows an example L-band HH-pol tomogram acquired by the tower. The canopy region of interest spans from 25 to 75 m in ground range and from 3 to 24 m in height. Within the region of interest, the horizontal (ground range) resolution ranges from 1.3 to 2.2 m and the vertical resolution ranges from 1.4 to 3.3 m, as numerically computed from point scatterer simulations. A canopy backscatter time series was produced by incoherently integrating the intensity over the region of interest. The produced canopy backscatter is of high precision with a

Fig. 1. BorealScat-2 radar tower (top), radar hardware rack (bottom left), and rendering of the tower top section with antenna array (bottom right). Functional details of the radar are described in [10].

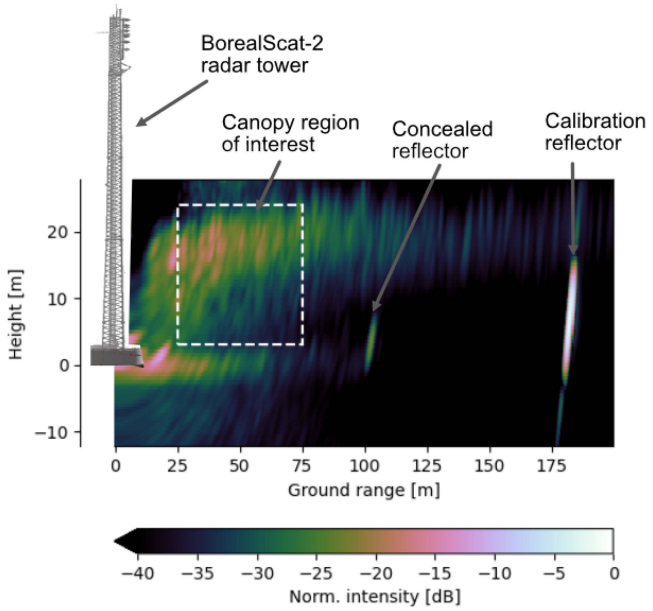

Fig. 2. Tomographic image at L-band, HH-pol acquired on 16 May 2024, at 14:23. Canopy region of interest and location of concealed (beneath canopy) and calibration (free line of sight) reflectors are highlighted.

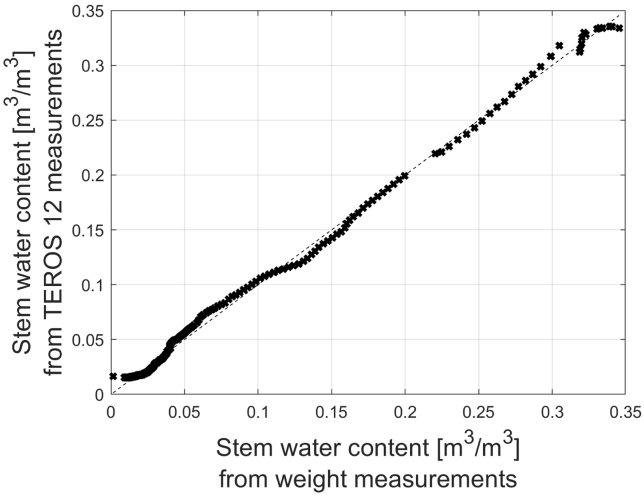

Fig. 3. StWC estimated from TEROS 12 sensor measurements when applying the calibration curve versus StWC estimated from gravimetric measurements. Each point represents the mean of the measured StWC taken from nine sampled trunk sections. The dashed line is a 1:1 reference line. The linear model yielded an R^2 of 0.998.

radiometric resolution better than 0.07 dB [10]. Radiometric resolution is here defined as the standard deviation of logarithmic backscatter under fully developed speckle conditions. Relative attenuation was estimated by extracting and inverting the peak backscatter value at VV and HH at the position of the CR shown in Fig. 2. Due to the high precision backscatter estimates, no smoothing over time was necessary to increase the number of independent samples. No absolute calibration of backscatter and attenuation time series was performed. Therefore, only the temporal variation of radar backscatter and attenuation will be investigated.

C. Ancillary Data

Meteorological data were acquired by the ICOS Svartberget Ecosystem Station [20]. From this dataset, soil water content (SWC) at 2.5 cm depth, precipitation and vapor pressure deficit (VPD) were used. VPD is a measure of the atmospheric demand of tree transpiration. VPD, which is a function of relative humidity and temperature of the air, is high during hot and dry conditions, often resulting in large variations in VWC.

Stem radius changes from eight trees within the radar footprint were measured using Natkon point dendrometers (ZN12-T-WP and ZN12-T-2WP) installed at breast height. Stem diameter time series of eight sensors were averaged to produce a single stem diameter time series representative of the radar footprint. Stem diameter shows variations due to both growth and subdaily water content variations [12].

StWC was measured in situ by TEROS 12 soil moisture sensors from METER Group. The TEROS 12 sensor is a capacitance-based sensor that measures the charging time of a capacitor, which depends on the dielectric permittivity of the surrounding material [21], [22]. When inserted in a tree stem, the dielectric permittivity is dominated by the volume fraction of liquid water [23], making the sensor suitable for estimating StWC.

To calibrate the raw sensor measurements for StWC a linear relationship between raw sensor outputs and volumetric StWC was applied. To obtain calibration constants, trunk sections of nine trees (three pine, three spruce, and three birch) were destructively sampled. The sampled trunk sections were dried and weighed in the laboratory while simultaneously acquiring raw sensor measurements with TEROS 12 sensors. A linear calibration curve was then applied to convert raw measurements to volumetric StWC. Fig. 3 shows the calibrated StWC sensor measurements versus the StWC measurements determined from weight measurements. The linear model yielded an R^2 of 0.998.

The TEROS 12 sensors were installed in tree trunks at breast height (1.35 m) and 8 m height (see Fig. 4) in eight trees within the radar footprint. Of the eight instrumented trees, only two (one pine and one spruce) had continuous, high-quality data that overlapped with the selected rain-free periods of interest. Thus, only the in situ StWC time series of these two trees are included in this study.

All ancillary data were interpolated and resampled to match the backscatter time series, allowing correlations between radar and ancillary variables to be investigated.

III. Methods

In the following section, a simplified scattering model relating canopy backscatter at L-band by the BorealScat 2 radar tower and VWC, is introduced. In addition, a model relating L-band attenuation and VWC is presented.

Fig. 4. StWC sensors (METER Group TEROS 12) installed at breast height (left) and at a height of 8 m (right) on pine trees.

A. Model

Several forest backscatter models are designed to relate backscatter and above-ground biomass (AGB) [16], [24], [25]. However, it is the water content within the biomass that predominantly influences the backscatter [26]. Therefore, establishing a direct relationship between backscatter and VWC is physically meaningful.

Existing forest backscatter models range from simplified scattering models to physically detailed multiple-scattering frameworks. Examples include the MIMICS model [27], the Tor Vergata model [28], and more recent developments that incorporate higher order scattering effects [29], [30]. These models require detailed structural information about the vegetation, such as stem diameter distributions, leaf orientation, and vegetation element density. In particular the spatial distribution of water content contained within the vegetation [31] is a necessary input as it directly influences the dielectric constant of the material and thus the backscattered signal.

Due to the absence of detailed structural forest data, a simplified modeling approach was adopted in this study. Moreover, we focus exclusively on canopy backscatter, with contributions from ground, double-bounce, and triple-bounce scattering removed by excluding intensity below 3 m height (see Fig. 2). Many of the improvements in recent models primarily improve estimates of scattering terms including the ground, which is not relevant in our case. In addition, we neglect multiple-scattering effects within the canopy, assuming that their influence is limited to an offset in dB and does not affect the relative variations in backscatter [29] as VWC variations are small (less than 10%).

In this study, we employ the single-scattering radiative transfer model, assuming a homogeneous vegetation canopy of height d with uniform attenuation and scattering properties. This simplification allows for tractable parameter estimation while retaining physical relevance. Notably, this model is equivalent to the solution derived from the distorted Born approximation, which is frequently employed in backscatter modeling [29].

Then, the canopy backscatter σ^0_{can} and the two-way attenuation L^2 through the full canopy can be modeled as [32]

$$\sigma^0_{\text{can},pq} = \frac{\sigma^{\text{back}}_{v,pq}\cos\theta_i}{\kappa_p+\kappa_q}\left(1-\exp\left(-\frac{(\kappa_p+\kappa_q)d}{\cos\theta_i}\right)\right) \quad (1)$$

$$L^2_{pq} = \exp\left(\frac{(\kappa_p+\kappa_q)d}{\cos\theta_i}\right) \quad (2)$$

where $\kappa[\text{m}^{-1}]$ is the extinction coefficient, $\sigma^{\text{back}}_v[\text{m}^{-1}]$ is the volume backscattering coefficient of the vegetation, and θ_i is the incidence angle. The indices p and q refer to the receive and transmit polarization.

Note that the product of the extinction coefficient and canopy height, $\kappa \cdot d$, corresponds to the vegetation optical depth (VOD), a parameter commonly retrieved from passive microwave remote sensing observations. The model presented in (1) thus highlights the connection of VOD to active microwave remote sensing observations.

A simplified model based on (1) is the water cloud model [15]. The water cloud model treats the canopy as a uniform volume-distributed cloud of Rayleigh scatterers, where both the volume backscattering coefficient and extinction coefficient are proportional to VWC [15]. Canopy backscatter in (1) is then related to VWC through the attenuation term, as the dependency on VWC in the scattering and extinction coefficients cancels out. Canopy backscatter is thus a monotonically increasing function of VWC.

However, previous observations from BorealScat-2 at L-band contradict this relationship [10]. L-band backscatter is observed to peak during the day [10], a time where VWC is expected to reach its minimum due to high transpirational rates depleting the internal water storage of trees [12]. This observation suggests a monotonically decreasing relationship between canopy backscatter and VWC, at least on diurnal time scales. The water cloud model which generally holds well for low vegetation canopies, such as crops [33], thus fails in the case of the boreal forest observed at L-band by BorealScat-2. The reason for this is, most likely, that the assumption of Rayleigh scatterers for forest canopy observations at L-band is generally not fulfilled, due to the presence of larger structures compared to crop vegetation.

Empirical and theoretical results have shown that a power law relationship can effectively describe the link between backscatter and AGB at P-band [17], [34]. Trong-Loï et al. [17] suggested the incorporation of a power law via the introduction of structural parameters when linking scattering and extinction coefficients to AGB. As we extract canopy backscatter in this study, only the volume scattering component of the Truong-Loï model is considered in the following. Furthermore, the canopy backscatter is expressed in terms of VWC $[\text{m}^3/\text{m}^3]$ instead of AGB, where VWC is the average volumetric water content contained in the volume spanned by vegetation ground area and canopy height d.

As Truong-Loi et al. [17] found the structural coefficient describing the relationship between AGB and attenuation to be $\beta = 1$ for all polarizations, we assume in the following $\kappa \propto$ VWC. Along the lines of the Truong-Loï model, assuming

$\sigma_v^{\text{back}} \propto \text{VWC}^{\alpha}$ the canopy backscatter can then be modeled as

$$\sigma^0_{\text{can},pq} = A_{pq} \cos\theta_i \text{VWC}^{\alpha_{pq}-1} \left(1 - \exp\left(-\frac{k_{pq}\text{VWC}}{\cos\theta_i}\right)\right) \tag{3}$$

where α and A are structural parameters that depend on size composition, dielectric constants, and orientation of the tree components and where k is a proportionality factor relating VWC to κd.

Likewise the two-way attenuation in (2) can in terms of VWC be modeled as

$$L^2_{pq} = \exp\left(\frac{k_{pq}\text{VWC}}{\cos\theta_i}\right). \tag{4}$$

B. Parameter Estimation

The VWC used in (3)–(4) is the average volumetric water content of the full vegetation layer in the region of interest. Sampling in the entire region of interest is not feasible. An alternative approach is to identify a tree water pool that best represents the changes in VWC in the region of interest.

Canopy backscatter is strongest in the upper canopy above 10 m in height (as shown in Fig. 2), and the most significant changes in backscatter occur in this layer [35]. Since changes in canopy backscatter are assumed to be due to variations in water content, canopy water content is considered to be the driving factor in VWC changes. Therefore, the upper canopy is likely the most representative water pool for VWC changes.

However, no water content measurements in the upper canopy were available. In this study, in situ StWC at 8 m height was assumed to be the most suitable for capturing changes in VWC, since it was the in situ StWC at the highest elevation available. Moreover, only the in situ StWC of the pine tree was used, as pine is the dominant species in the area of interest and therefore considered the most representative.

Three rain free time periods in 2024 during which clear diurnal cycles in backscatter and attenuation occurred were chosen for parameter estimation.

1) P_1: 14–25 May.
2) P_2: 27 May to 3 June.
3) P_3: 5–9 June.

Parameter estimation was performed at all three polarization combinations across all time periods.

Structural coefficients and additional calibration coefficients in (3) and (4) were estimated separately. Two radar estimated StWC time series per polarization were extracted from attenuation and canopy backscatter, respectively. The parameter estimation process for the canopy backscatter and attenuation models is described as follows.

1) Canopy Backscatter: The BorealScat-2 radar tower provides tomographic measurements, enabling the separation of backscatter contributions from different height layers of the forest, particularly from canopy and ground level backscatter. Within the canopy region of interest the incidence angle θ_i in (3) varies within $[26.6^{\text{o}}, 56.3^{\text{o}}]$. It is expressed as an effective angle of $\theta_i = 51^{\text{o}}$ which is the incidence angle at the main intensity peak within the canopy region of interest shown in Fig. 2.

Proportionality between model VWC in the canopy region of interest and in situ measured StWC of a pine tree at 8 m height is assumed with an unknown proportionality factor that is captured by k_{pq} in (3). Note that in this study it is assumed that canopy water content can be approximated from StWC measurements from a single point within a tree. This approach relies on the assumption that scaling from the single tree level to the stand level can be represented by a simple proportional relationship. In addition, potential temporal lags between water content changes in upper and lower canopy [36], [37] are not explicitly accounted for. These simplifications may introduce uncertainty and should be considered as limitations of the current modeling approach.

Canopy backscatter can then directly be modeled from in situ StWC. Structural coefficients α_{pq}, A_{pq} and, up to a scaling factor, k_{pq} given in (3) are estimated by minimizing the sum of the mean squared errors between modeled and measured canopy backscatter over the time period of interest. MATLAB's "lsqnonlin" function with a Levenberg–Marquardt algorithm, combined with a Monte-Carlo simulation of the initial parameters, was used to minimize the cost function.

2) Attenuation: The CR used in this study for attenuation measurements was not absolutely calibrated, thus an additional unknown calibration factor is included in the parameter estimation process. Cross-polarized attenuation is approximated as

$$L^2_{vh} = \sqrt{L^2_{hh} \cdot L^2_{vv}}. \tag{5}$$

The incidence angle at the CR is $\theta_R = 61.7^{\text{o}}$. Proportionality between model VWC in the line of sight of the CR and in situ measured StWC is assumed with an unknown proportionality factor that is captured by k_{pq} in (4). Here, it is assumed that single tree StWC can represent VWC along the reflectors line of sight neglecting possible temporal lags between StWC and water content that the radar is sensitive to. Linear regression is performed between in situ measured StWC and logarithmic relative attenuation in order to determine the unknown calibration constant and k_{pq} in (4).

IV. Results

A. Time Series Observations

Fig. 5 shows the measured canopy backscatter time series at VV, HH, and cross-polarizations, along with measurements of attenuation at VV and HH during the chosen rain-free periods used in this study and measurements of StWC of a pine and a spruce tree. Clear diurnal cycles in canopy backscatter (about 0.5 dB min to max) and attenuation (up to 2 dB for VV and 1 dB for HH min to max) are observed at all polarization combinations. Backscatter has maxima during the middle of the day and minima during the nights, whereas attenuation reaches minima in the middle of the day and maxima during nights. During 19 to 21 May for an unknown reason, the average backscatter drops about 0.3 dB, whereas no clear change in average attenuation is observed during those days. From 27 May onwards, average VV attenuation increases constantly until the end of the observation period (2 dB). HH average attenuation increases only slightly

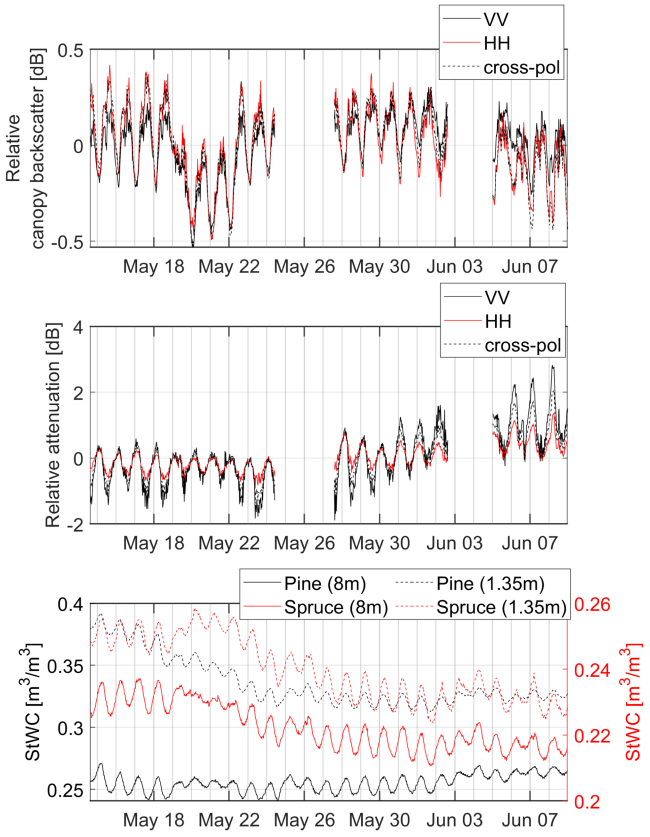

Fig. 5. Measured relative canopy backscatter (top) and attenuation (middle) at VV, HH, and cross-pol during rain free time periods in 2024. StWC from a pine tree and a spruce tree at 8 m height and breast height (1.35 m) that lie within the foot print of the radar tower (bottom). The vertical grid lines coincide with midnights.

(1 dB) during that time period. Average canopy backscatter at all polarizations decreases constantly after the 27 May (about 0.5 dB). Concerning the StWC measurements, clear diurnal cycles are observed for both trees at both measurement heights.

From these observations, an upper bound of the structural coefficient α can be formulated. As canopy backscatter peaks in the middle of the day and has minima during the night, a pattern opposite to the diurnal cycle of StWC, which peaks at night and is lowest during the day, is observed. Only an α coefficient that is smaller than 1 can capture this behavior.

B. Model Parameter Estimation

During the parameter estimation process for the canopy backscatter, it became apparent that no clear minima in the cost function for a fixed structural coefficient α could be identified. Fig. 6 shows the models root-mean-squared error (RMSE) as a function of α. No clear minima in RMSE are found for each polarization, indicating that no unique solution for α exists. Instead, a broad range of α values provides acceptable model solutions. Table I lists the range of α values for which RMSE between modeled and measured backscatter deviates less than 5% from the minimal RMSE. These α ranges span between $\alpha = -1.3$ and $\alpha = 0.8$ depending on the polarization used.

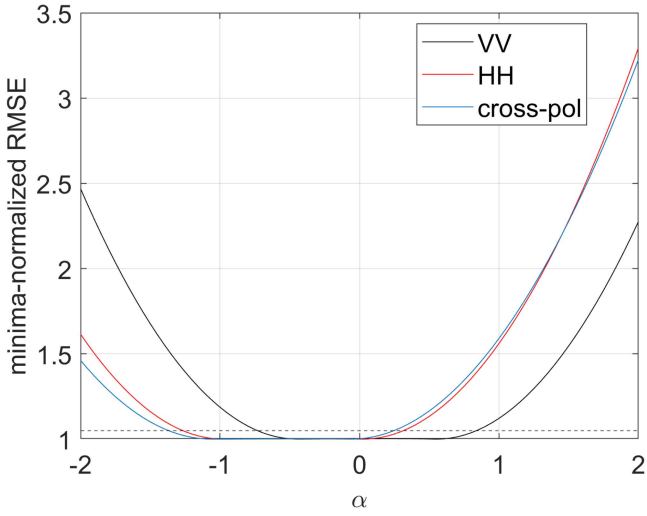

Fig. 6. Sensitivity plot of α. The RMSE is normalized by the minimal RMSE for each polarization, respectively. The dashed horizontal line indicates the RMSE that deviates 5% from the minimal RMSE.

TABLE I
RANGES OF α COEFFICIENTS FOR WHICH THE RMSE BETWEEN MODELED AND MEASURED BACKSCATTER DEVIATES LESS THAN 5% FROM THE MINIMAL RMSE SHOWN IN FIG. 6

	$\alpha_{\min}$	$\alpha_{\max}$
VV	−0.7	0.8
HH	−1.2	0.3
cross-pol	−1.3	0.2

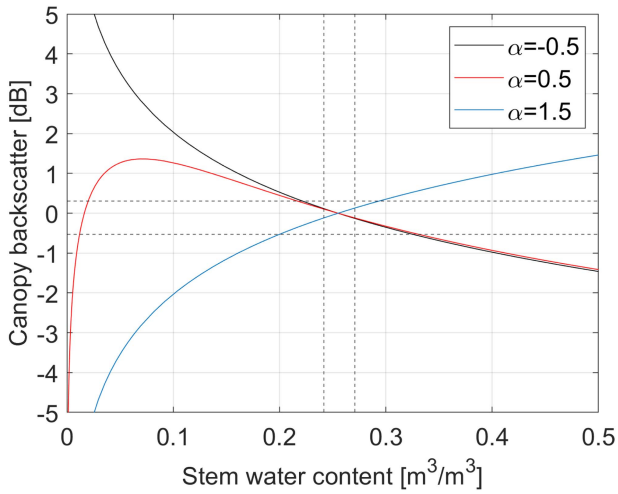

Fig. 7. Canopy backscatter at VV using the estimated coefficients in (3) for fixed α values. Dashed horizontal lines mark the lower and upper limit for the canopy backscatter used during the parameter estimation process. Dashed vertical lines indicate the lower and upper limit for the StWC used during the parameter estimation process.

Fig. 7 shows the canopy backscatter as a function of model StWC for different structural coefficients α. Functions for other α values show the same behavior as the three chosen α values. For $\alpha \leq 0$, canopy backscatter is monotonically decreasing with StWC. For $0 < \alpha < 1$, canopy backscatter increases with

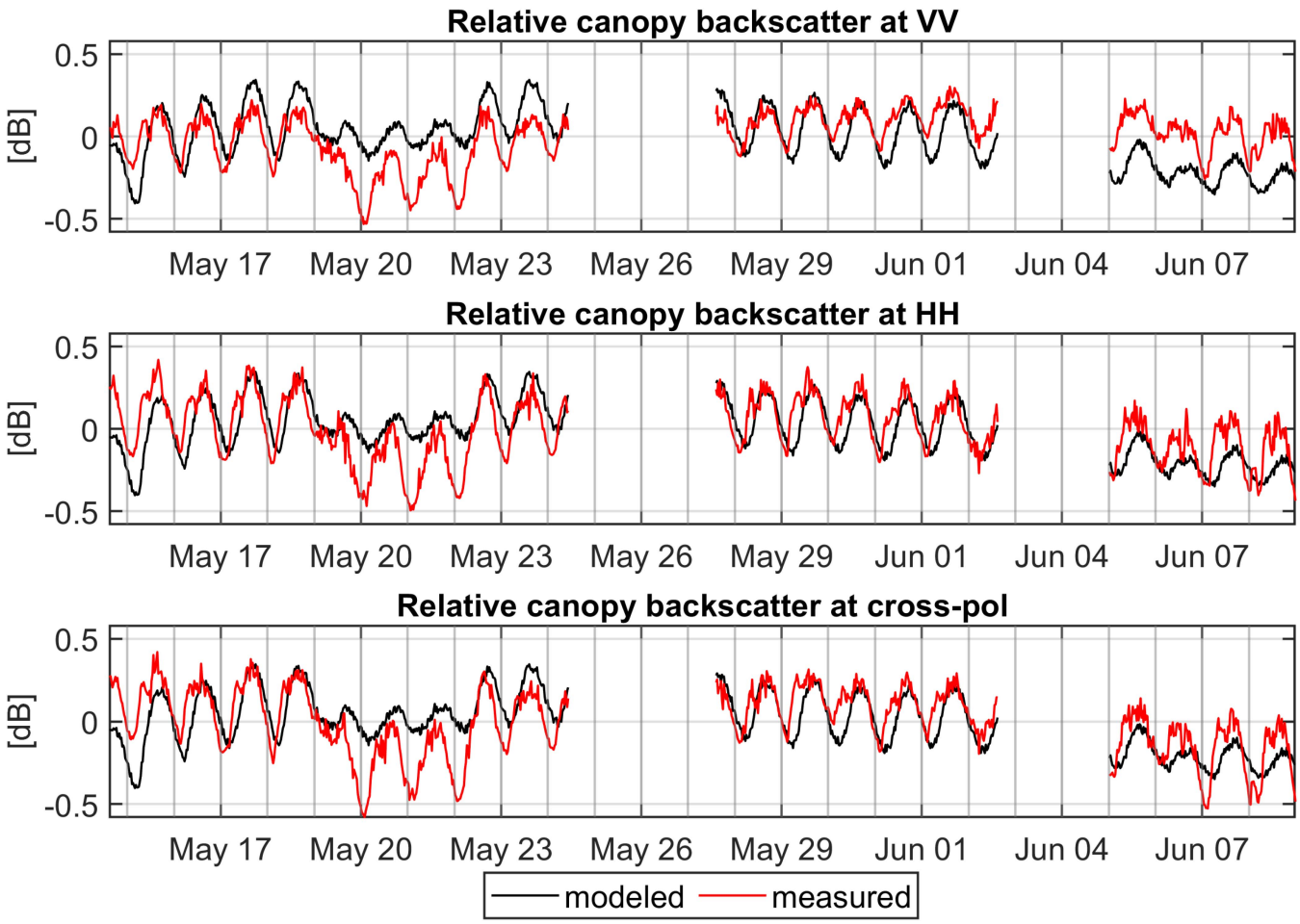

Fig. 8. Measured and modeled canopy backscatter at all polarization combinations. Modeled canopy backscatter is computed from in situ StWC and model coefficients estimated by minimizing the RMSE. The vertical grid lines coincide with midnight.

StWC, then reaches a maximum, and decreases monotonically for higher StWC values. For $\alpha \geq 1$, canopy backscatter is a monotonically increasing function with StWC. This also illustrates why a broad range of α values provides acceptable model solutions. The global function behavior varies for different α coefficients over a wide range of StWC values. However, within the specific range of StWC and canopy backscatter for which the parameters were estimated, different $\alpha < 1$ are able to capture the same relationship between backscatter and StWC.

In the following, $\alpha = 0$ is chosen as a fixed structural coefficient for all polarizations, as all α values within the ranges listed in Table I show similar trends in StWC and backscatter.

Fig. 8 shows the measured and modeled canopy backscatter at all polarization combinations. The modeled canopy backscatter time series follows the measured canopy backscatter well, capturing the diurnal variations and long-term trends. However, the clear drop in mean canopy backscatter during 19–22 May could not be captured by the model which during this time shows a decrease in the strength of the diurnal variation. In addition, a phase shift of 2.5 h is observed between modeled and measured canopy backscatter. This phase shift is addressed in more detail in Section V.

For all polarization combinations, StWC time series were produced by inverting canopy backscatter and attenuation to StWC using the estimated model parameters.

Fig. 9 presents the estimated StWC time series derived from canopy backscatter (top panel) and attenuation (second panel) at all polarizations, alongside in situ StWC. StWC modeled from inversion of canopy backscatter from all polarizations show a similar behavior. Clear diurnal cycles are observed in both modeled and measured StWC. Diurnal maxima in StWC occur at night, coinciding with maxima in stem radius and minima in VPD, whereas diurnal minima in StWC align with peak VPD and minima in stem radius. This is expected, as high VPD leads to higher transpiration, depleting tree internal water reserves and thus decreasing StWC. Between 19 and 21 May modeled StWC is overestimated in comparison to in situ StWC. During this time period a drop in VPD is observed along with a minimal rain event (0.1 mm). Beyond this period, average modeled and measured StWC increased steadily, likely due to the two significant rain events recorded in May and June. This increase contrasts with SWC, which shows a decreasing trend over the same period. Modeled and measured StWC align well, with an RMSE around 4% for all polarizations.

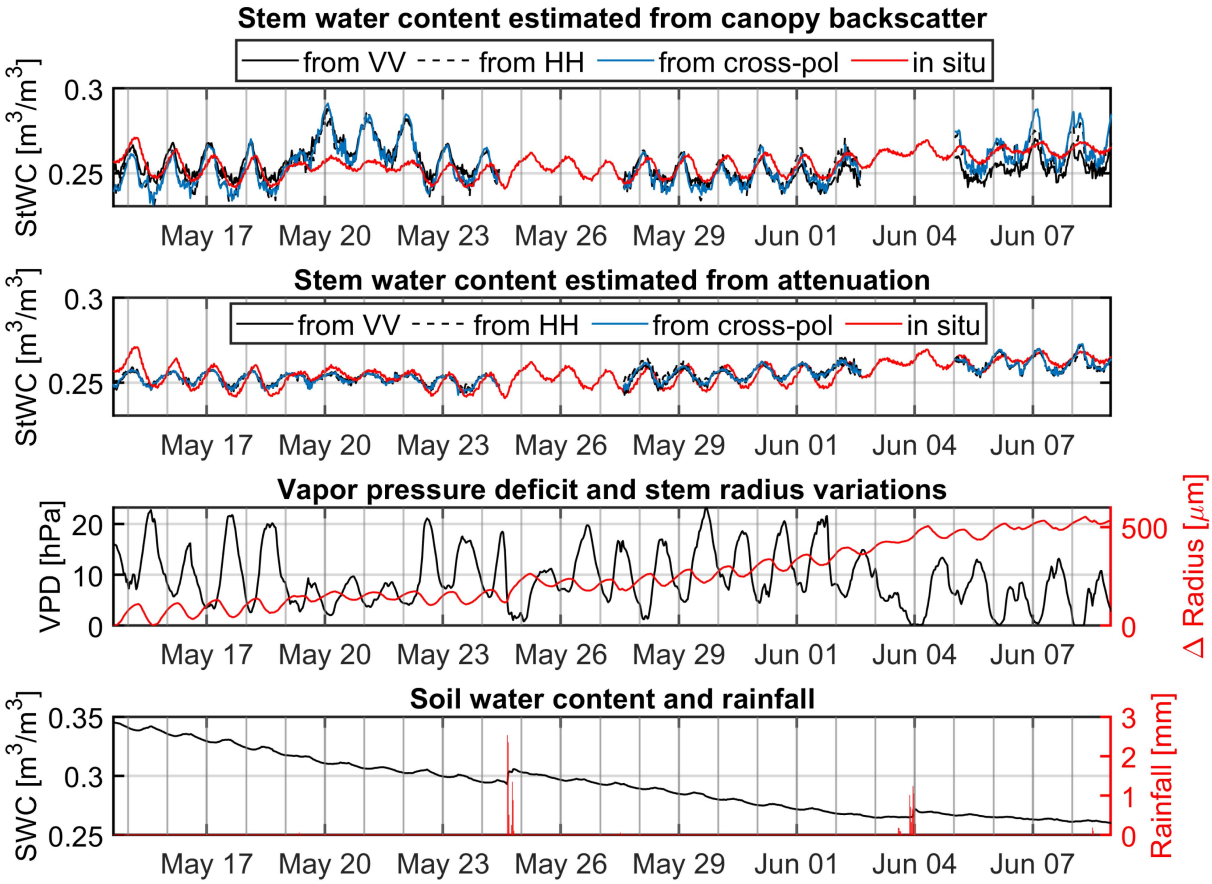

Fig. 9. StWC modeled from canopy backscatter (top panel, assuming $\alpha = 0$) and attenuation (second panel) at all polarizations alongside in situ StWC. The lower two panels show VPD, stem radius changes, SWC, and precipitation data. The vertical grid lines coincide with midnight.

The estimated StWC time series obtained from attenuation at all polarizations show excellent agreement between diurnal fluctuations in modeled and in situ StWC during the full observation time period. Long-term trends in modeled StWC also align well with those in measured StWC, with an RMSE around 2% for all polarizations.

For both backscatter- and attenuation-estimated StWC, a phase shift of 2–2.5 h is observed relative to in situ StWC, as determined by a cross-correlation analysis. This phase shift likely arises because the attenuation-sensitive water pools (upper canopy and smaller branches) exhibit different water dynamics than the StWC measured in situ.

Overall, both modeled StWC changes capture the diurnal cycles. Apart from a few days for canopy backscatter estimated StWC, the modeled StWC estimates also reproduce long-term trends in measured StWC.

V. Discussion

This study aimed to establish a link between VWC and L-band radar backscatter using a simplified scattering model based on [17]. Time series of canopy backscatter were connected to in situ StWC measurements through three structural coefficients. The parameter estimation process identified a broad range of structural coefficient values, with acceptable solutions for α spanning from $-1.3 < \alpha < 0.8$. Different α values describe distinct relationships between VWC and canopy backscatter: for $\alpha < 0$, canopy backscatter monotonically decreases with VWC, whereas for $\alpha > 1$, it increases monotonically. For $0 < \alpha < 1$ a maxima in canopy backscatter for a certain VWC values occurs, a behavior that potentially could explain contradicting diurnal backscatter variations observed at different sites [10], [35].

Observations show that $\alpha < 1$ must be satisfied to yield realistic StWC estimates for this study site and period. This indicates that the ratio between volume backscattering coefficient and extinction coefficient is anticorrelated with StWC (see Fig. 7). The modeled and measured StWC aligned well over the full observation period, with an RMSE of 4% corresponding to $\alpha = 0$.

However, during a three-day period the average canopy backscatter slightly decreased, leading to an overestimation of backscatter-derived StWC. During this time period no changes in mean attenuation were observed and attenuation-derived StWC aligned well with measurements, with an RMSE of 2%. This period coincided with a significant drop in mean temperature of approximately 9° C, although temperatures remained above freezing. This temperature drop persisted until the end of the three-day period, after which temperatures rose again, and the average canopy backscatter increased. The cause of the drop in canopy backscatter is unclear. Time series of the vertical center of mass of backscatter showed no significant deviation during this period compared to the times before and after the

backscatter drop, suggesting no vertical redistribution of water content within the trees. It is hypothesized that a horizontal redistribution of water content may have occurred, affecting the scattering properties but not the attenuation.

The results demonstrate that variations in canopy backscatter observed at L-band by the BorealScat-2 experiment can be effectively captured by the proposed model and that the inversion of canopy backscatter to VWC is feasible. Furthermore, this study highlights that StWC extracted from attenuation inversion provides an even more accurate estimate, as in situ StWC measurements exhibited better agreement with attenuation-derived StWC than with backscatter-derived StWC.

A phase shift between modeled and measured StWC as well as between modeled and measured canopy backscatter was observed, likely, due to the fact that the water pool that the radar is sensitive to represents a different tree water pool than the measured upper StWC. It is assumed that canopy backscatter and attenuation are more sensitive to water pools that lie higher up in the tree (smaller branches). Those water pools are expected to be depleted earlier in the day than stem water pools as they are earlier affected by the onset of transpiration.

Several limitations need to be addressed in future research. The lack of a unique solution for α suggests that further refinement and calibration of the backscatter model are necessary. Future studies could address this by incorporating longer time series including a wider range of StWC and canopy backscatter observations, additional study sites, and an absolute calibration of the attenuation to constrain the model parameters more effectively. In addition, more dielectric sensors, e.g., higher up in the tree canopy could be installed. The observed phase shift between modeled and measured StWC also highlights the need for more detailed validation data to identify the specific water pools to which L-band backscatter is sensitive.

A. Relevance to Spaceborne SAR Missions

While this study is based on a limited in situ experiment using a simplified single-scattering model, it offers preliminary insights into the observational requirements for future spaceborne SAR missions aimed at retrieving forest VWC.

Tomographic SAR systems, such as the BorealScat-2 tower experiment, provide vertical resolution that allows for the isolation of canopy backscatter, conveniently separating vegetation water dynamics from soil moisture dynamics. Translating this capability to spaceborne platforms is challenging due to the spatial and temporal diversity required for subdaily tomographic observations. ESA's BIOMASS mission, operating at P-band and launched recently, is the first spaceborne SAR system with systematic tomographic capabilities [34]. It uses repeat-pass tomography, collecting multiple baselines over a relatively short time frame of 18 days. At L-band, repeat-pass tomography has been demonstrated using SAOCOM data [38] over a time frame of two months.

Since forest VWC varies on subdaily timescales, repeat-pass approaches with revisit intervals of several days are insufficient for capturing diurnal dynamics. Single-pass tomography at L-band would be ideal but is not feasible with current or planned satellite architectures.

An alternative to instantaneous tomography is single-pass interferometry, which could enable the suppression of ground contributions [39]. This potentially would enable long-term VWC changes to be estimated. Although no current mission offers zero temporal baseline interferometry at L-band, a proposed companion satellite [40] to ESA's ROSE-L mission (planned for launch in 2028) could provide this capability.

An alternative to tomography and single-pass interferometry is to model and subtract ground backscatter. This will introduce additional uncertainty and complexity, especially in dense forest environments, but is worth pursuing in future studies. Even if canopy only backscatter could be isolated in single SAR images, high temporal resolution remains essential for capturing subdaily dynamics.

This study demonstrates that diurnal cycles in backscatter and StWC are clearly observable, implying that a revisit time of less than 24 h is necessary to resolve these dynamics. The SLAINTE mission concept [41] aims to address this need by deploying a constellation of L-band SAR satellites capable of sampling the Earth up to three times per day. Combined with methods to isolate canopy backscatter, such a system could potentially enable operational monitoring of forest water content, including its diurnal variability.

VI. Conclusion

This study provides preliminary evidence that time series of tomographic L-band radar backscatter can be linked to StWC in a boreal forest. Observations of in situ StWC suggest that the ratio between volume backscattering coefficient and extinction coefficient is anticorrelated to VWC. The backscatter-derived StWC aligns well with diurnal and long-term trends observed in measured StWC, although a phase shift suggests that L-band backscatter is more sensitive to water pools in the upper canopy than to trunk water reserves. The attenuation-derived StWC provides an even better alignment with the measured data. These results indicate that forest VWC estimation is feasible using tomographic L-band radar platforms, offering a promising approach for monitoring forest hydrodynamics at large scales. While this study is based on tower-based observations and a simplified single-scattering model, these results offer initial insight into the observational requirements for future spaceborne SAR missions. In particular, they suggest that vertical separation of canopy and ground backscatter, achievable through tomography or interferometry, and subdaily temporal resolution may be important for capturing diurnal VWC dynamics. Further studies with more comprehensive datasets and refined models are needed to validate and generalize these findings.

Acknowledgment

The 5-meter trihedral corner reflectors were supplied and installed by the Swedish Defence Research Agency (FOI).

REFERENCES

[1] Y. Pan et al., "The enduring world forest carbon sink," *Nature*, vol. 631, pp. 563–569, Jul. 2024.

[2] D. Sheil, "Forests, atmospheric water and an uncertain future: The new biology of the global water cycle (in forest ecosystems)," *Forest Ecosystems*, vol. 5, pp. 1–22, Mar. 2018.

[3] T. Farooqi, R. Portela, Z. Xu, S. Pan, M. Irfan, and A. Ali, "Advancing forest hydrological research: Exploring global research trends and future directions through scientometric analysis," *J. Forestry Res.*, vol. 35, Sep. 2024, Art. no. 16.

[4] L. M. H. Ulander, A. R. Monteith, H. J. Persson, and J. E. S. Fransson, "Borealscat-2: Backscatter measurements of forest water dynamics," in *Proc. 2024 IEEE Int. Geosci. Remote Sens. Symp.*, Athens, Greece, Jul. 2024, pp. 2332–2335.

[5] C. Albinet et al., "TropiSCAT: A ground based polarimetric scatterometer experiment in tropical forests," *IEEE J. Sel. Topics Appl. Earth Observ. Remote Sens.*, vol. 5, no. 3, pp. 1060–1066, Jun. 2012.

[6] C. Albinet et al., "First results of AfriScat, a tower-based radar experiment in african forest," in *Proc. IEEE Int. Geosci. Remote Sens. Symp.*, Milan, Italy, Jun. 2015, pp. 5356–5358.

[7] S. El Idrissi Essebtey et al., "Temporal decorrelation of tropical dense forest at C-band: First insights from the TropiScat-2 experiment," *IEEE Geosci. Remote Sens. Lett.*, vol. 17, no. 6, pp. 928–932, Jun. 2020.

[8] A. R. Monteith and L. M. H. Ulander, "Temporal characteristics of P-band tomographic radar backscatter of a boreal forest," *IEEE J. Sel. Topics Appl. Earth Observ. Remote Sens.*, vol. 14, pp. 1967–1984, 2021.

[9] L. M. H. Ulander and A. R. Monteith, "BorealScat contract change notice 1 final report," European Space Agency (ESA), Tech. Rep. Contract 4000118576/16/NL/FF/mg, Mar. 2022. [Online]. Available: https://earth.esa.int/eogateway/campaigns/borealscat

[10] A. R. Monteith et al., "A tower-based radar experiment for studying the effects of boreal forest tree-water relations," *SSRN Electron. J.*, Oct. 2024. [Online]. Available: http://dx.doi.org/10.2139/ssrn.4991471

[11] D. Whitehead, and P. Jarvis, "Coniferous forests and plantations," in *Woody Plant Communities*. New York, Ny, USA: Academic Press, 1981.

[12] R. Zweifel, H. Item, and R. Häsler, "Link between diurnal stem radius changes and tree water relations," *Tree Physiol.*, vol. 21, no. 12–13, pp. 869–877, Aug. 2001.

[13] S. Pfautsch, J. Renard, M. G. Tjoelker, and A. Salih, "Phloem as capacitor: Radial transfer of water into xylem of tree stems occurs via symplastic transport in ray parenchyma," *Plant Physiol.*, vol. 167, no. 3, pp. 963–971, Jan. 2015.

[14] P. C. Vermunt, S. C. Steele-Dunne, S. Khabbazan, J. Judge, and N. C. van de Giesen, "Extrapolating continuous vegetation water content to understand sub-daily backscatter variations," *Hydrol. Earth System Sci.*, vol. 26, no. 5, pp. 1223–1241, Mar. 2022.

[15] E. P. Attema and F. T. Ulaby, "Vegetation modeled as a water cloud," *Radio Sci.*, vol. 13, pp. 357–364, Mar. 1978.

[16] J. I. Askne, M. J. Soja, and L. M. H. Ulander, "Biomass estimation in a boreal forest from TanDEM-X data, LiDAR DTM, and the interferometric water cloud model," *Remote Sens. Environ.*, vol. 196, pp. 265–278, Jul. 2017.

[17] M.-L. Truong-Loi, S. Saatchi, and S. Jaruwatanadilok, "Soil moisture estimation under tropical forests using UHF radar polarimetry," *IEEE Trans. Geosci. Remote Sens.*, vol. 53, no. 4, pp. 1718–1727, Apr. 2015.

[18] S. S. Saatchi and M. Moghaddam, "Estimation of crown and stem water content and biomass of boreal forest using polarimetric SAR imagery," *IEEE Trans. Geosci. Remote Sens.*, vol. 38, no. 2, pp. 697–709, Mar. 2000.

[19] J. Chi et al., "The net landscape carbon balance—integrating terrestrial and aquatic carbon fluxes in a managed boreal forest landscape in Sweden," *Glob. Change Biol.*, vol. 26, no. 4, pp. 2353–2367, Jan. 2020.

[20] M. Peichl et al., "ETC L2 ARCHIVE, svartberget, 2019-01-01–2024-09-01," 2024. [Online]. Available: https://hdl.handle.net/11676/aji8KUPQYA4MeDyJBWRnRx0S

[21] METER Group, Inc., "TEROS 11/12 user manual," Pullman, WA, USA, 2024, Accessed: Jun. 19, 2025. [Online]. Available: https://publications.metergroup.com/Manuals/20587_TEROS11-12_Manual_Web.pdf

[22] T. H. Lo et al., "Field assessment of interreplicate variability from eight electromagnetic soil moisture sensors," *Agricultural Water Manage.*, vol. 231, 2020, Art. no. 105984.

[23] G. Torgovnikov, *Dielectric Properties of Wood and Wood-Based Materials*. Berlin, Germany: Springer Ser. Wood Sci., Jan. 1993.

[24] M. J. Soja et al., "Mapping above-ground biomass in tropical forests with ground-cancelled P-band SAR and limited reference data," *Remote Sens. Environ.*, vol. 253, 2021, Art. no. 112153. [Online]. Available: https://www.sciencedirect.com/science/article/pii/S0034425720305265

[25] A. Toraño Caicoya, M. Pardini, I. Hajnsek, and K. Papathanassiou, "Forest above-ground biomass estimation from vertical reflectivity profiles at L-band," *IEEE Geosci. Remote Sens. Lett.*, vol. 12, no. 12, pp. 2379–2383, Dec. 2015.

[26] A. Konings et al., "Detecting forest response to droughts with global observations of vegetation water content," *Glob. Change Biol.*, vol. 27, pp. 6005–6024, Sep. 2021.

[27] F. T. Ulaby, K. Sarabandi, K. McDonald, M. Whitt, and M. C. Dobson, "Michigan microwave canopy scattering model," *Int. J. Remote Sens.*, vol. 11, no. 7, pp. 1223–1253, 1990.

[28] M. Link, T. Jagdhuber, P. Ferrazzoli, L. Guerriero, and D. Entekhabi, "Relationship between active and passive microwave signals over vegetated surfaces," *IEEE Trans. Geosci. Remote Sens.*, vol. 60, 2022, Art. no. 5301715.

[29] M. Salim, S. Tan, R. D. De Roo, A. Colliander, and K. Sarabandi, "Passive and active multiple scattering of forests using radiative transfer theory with an iterative approach and cyclical corrections," *IEEE Trans. Geosci. Remote Sens.*, vol. 60, 2022, Art. no. 4402916.

[30] L. Tsang, J. A. Kong, and R. T. Shin, *Theory of Microwave Remote Sensing*. New York, NY, USA: Wiley, 1985.

[31] M. Kravka, T. Krejzar, and J. Čermák, "Water content in stem wood of large pine and spruce trees in natural forests in central Sweden," *Agricultural Forest Meteorol.*, vol. 98–99, pp. 555–562, Dec. 1999. [Online]. Available: https://www.sciencedirect.com/science/article/pii/S0168192399001239

[32] F. T. Ulaby and D. G. Long, *Microwave Radar and Radiometric Remote Sensing*. Ann Arbor, MI, USA: Univ. Michigan Press, 2014.

[33] P. C. Vermunt, S. C. Steele-Dunne, S. Khabbazan, V. Kumar, and J. Judge, "Towards understanding the influence of vertical water distribution on radar backscatter from vegetation using a multi-layer water cloud model," *Remote Sens.*, vol. 14, no. 16, Aug. 2022, Art. no. 3867.

[34] S. Quegan et al., "The European space agency biomass mission: Measuring forest above-ground biomass from space," *Remote Sens. Environ.*, vol. 227, pp. 44–60, Jun. 2019. [Online]. Available: https://www.sciencedirect.com/science/article/pii/S0034425719301233

[35] P. J. Bennet, A. R. Monteith, and L. M. H. Ulander, "Diurnal cycles of L-band tomographic SAR backscatter in a boreal forest during summer: Observations by the borealscat tower radar," in *Proc. 2023 IEEE Int. Geosci. Remote Sens. Symp.*, Pasadena, CA, USA, Jul. 2023, pp. 2195–2198.

[36] J. Cermák, J. Kučera, W. Bauerle, N. Phillips, and T. Hinckley, "Tree water storage and its diurnal dynamics related to sap flow and changes in stem volume in old-growth douglas-fir trees," *Tree Physiol.*, vol. 27, pp. 181–98, Mar. 2007.

[37] Y. Preisler et al., "The importance of tree internal water storage under drought conditions," *Tree Physiol.*, vol. 42, pp. 771–783, Nov. 2021.

[38] F. Banda, N. Petrushevsky, S. Tebaldini, and A. Monti-Guarnieri, "Demonstration of spaceborne L-band forest SAR tomography with SAOCOM," *IEEE Trans. Geosci. Remote Sens.*, vol. 63, 2025, Art. no. 5208611.

[39] M. Mariotti d'Alessandro, S. Tebaldini, S. Quegan, M. J. Soja, L. M. H. Ulander, and K. Scipal, "Interferometric ground cancellation for above ground biomass estimation," *IEEE Trans. Geosci. Remote Sens.*, vol. 58, no. 9, pp. 6410–6419, Sep. 2020.

[40] M. Bachmann et al., "ROSE-L tandem–bistatic extension for single-pass interferometry," in *Proc. EUSAR 2022; 14th Eur. Conf. Synthetic Aperture Radar*, 2022, pp. 1–4.

[41] S. Steele-Dunne et al., "SLAINTE: A SAR mission concept for sub-daily microwave remote sensing of vegetation," in *Proc. EUSAR 2024; 15th Eur. Conf. Synthetic Aperture Radar*, 2024, pp. 870–872.

Theresa Leistner received the M.Sc. degree in physics from Leipzig University, Leipzig, Germany, in 2021. She is currently working toward the Ph.D. degree in radio and space science with the Department of Space, Earth, and Environment, Chalmers University of Technology, Gothenburg, Sweden.

Her research focuses on radar remote sensing of forests.

Albert R. Monteith (Member, IEEE) received the M.Sc. degree in electrical engineering and the Ph.D. degree in radio and space science from the Chalmers University of Technology, Gothenburg, Sweden, in 2015 and 2020, respectively.

He is currently a Research Specialist with the Department of Space, Earth, and Environment, Chalmers University of Technology. His research interests include the temporal aspects of radar remote sensing of forests and in the development of new radar instruments and algorithms for remote sensing applications.

Jose Gutierrez Lopez received the Ph.D. degree in natural resources and environmental sciences from the University of New Hampshire, Durham, NH, USA, in 2019.

He is currently a Researcher with the Department of Forest Ecology and Management, Swedish University of Agricultural Sciences. His research interests include the links between tree physiology and forest management, with a strong emphasis on plant water use and water yield. His current work is focused on the use and development of in situ sensors for characterizing the water status of forests for studying tree water use and drought response.

Lars M. H. Ulander (Fellow, IEEE) received the M.Sc. degree in engineering physics and the Ph.D. degree in electrical and computer engineering from the Chalmers University of Technology, Gothenburg, Sweden, in 1985 and 1991, respectively.

Since 1995, he has been with Swedish Defence Research Agency (FOI), where he is the Director of research in radar signal processing and leads the research on very high frequency/ultrahigh frequency band radar. Since 2014, he has been a Professor in radar remote sensing with the Chalmers University of Technology. He has authored or coauthored more than 300 professional publications, of which more than 60 are in peer-reviewed scientific journals. He is the holder of five patents. His research interests include synthetic aperture radar, electromagnetic scattering models, and remote sensing applications.